The Astrophysical Journal, 961:215 (12pp), 2024 February 1 https://doi.org/10.3847/1538-4357/ad1605

Between the Cosmic-Ray "Knee" and the "Ankle": Contribution from Star Clusters

Sourav Bhadra[1,2], Satyendra Thoudam[3], Biman B Nath[1], and Prateek Sharma[2]
[1] Raman Research Institute, Sadashiva Nagar, Bangalore 560080, India
[2] Joint Astronomy Programme, Department of Physics, Indian Institute of Science, Bangalore 560012, India
[3] Department of Physics, Khalifa University, PO Box 127788, Abu Dhabi, United Arab Emirates
Received 2023 September 7; revised 2023 November 30; accepted 2023 December 11; published 2024 January 29

Abstract

We show that massive, young star clusters may be possible candidates that can accelerate Galactic cosmic rays (CRs) in the range of 10^7–10^9 GeV (between the "knee" and "ankle"). Various plausible scenarios, such as acceleration at the wind termination shock and supernova shocks inside these young star clusters, have been proposed, since it is difficult to accelerate particles up to the 10^7–10^9 GeV range in the standard paradigm of CR acceleration in supernova remnants. We consider a model for the production of different nuclei in CRs from massive stellar winds using the observed distribution of young star clusters in the Galactic plane. We present a detailed calculation of CR transport in the Galaxy, taking into account the effect of diffusion, interaction losses during propagation, and particle reacceleration by old supernova remnants to determine the all-particle CR spectrum. Using the maximum energy estimate from the Hillas criterion, we argue that a young, massive star cluster can accelerate protons up to a few tens of PeV. Upon comparison with the observed data, our model requires a CR source spectrum with an exponential cutoff of $5 \times 10^7 Z$ GeV ($50\,Z$ PeV) from these clusters, together with a CR injection fraction of ∼5% of the wind kinetic energy. We discuss the possibility of achieving these requirements in star clusters, as well as the associated uncertainties, in the context of considering star clusters as the natural accelerator of the "second component" of Galactic CRs.

Unified Astronomy Thesaurus concepts: Cosmic rays (329); Particle astrophysics (96); High energy astrophysics (739); Galactic cosmic rays (567); Young star clusters (1833)

1. Introduction

Cosmic rays (CRs) are high-energy particles that span an extensive range of energy from 1 to $\sim 10^{11}$ GeV. Lower-energy CRs up to $\sim 10^5$–10^6 GeV are believed to be accelerated by supernova (SN) shocks (Lagage & Cesarsky 1983; Axford 1994). This dominant acceleration mechanism, revealed by both theoretical (Fermi 1949; Axford et al. 1977; Bell 1978; Blandford & Ostriker 1978; Blasi 2013; Caprioli 2015) and observational (Drury et al. 1994; Ackermann et al. 2013; H. E. S. S. Collaboration et al. 2018) studies, is diffusive shock acceleration (DSA), a first-order Fermi acceleration process in which ∼10% of the shock energy is expected to be converted to CRs. Although the acceleration mechanism continues to work throughout the active stage of a supernova remnant (SNR) until it becomes indistinguishable from the ambient interstellar medium after $\sim 10^5$–10^6 yr, most of the particle acceleration occurs during the undecelerated blast wave phase, which lasts for $\leqslant 10^3$ yr (Lagage & Cesarsky 1983). This limits the maximum CR energy that can be accelerated in SNRs because the acceleration time of CR particles cannot be longer than the age of the SNR (Morlino 2017). Considering nonlinear effects such as the scattering of the CRs by the waves they generate themselves and assuming the magnetic flux density of the interstellar magnetic field to be $\sim\mu$G, Lagage & Cesarsky (1983) estimated the upper limit of CR energy in SNRs to be $\sim 10^5$ GeV nucleon^{-1}.

These theoretical ideas have found observational confirmation. Suzuki et al. (2022) reported cutoff energy of around TeV from γ-ray observations of 15 SNRs. Recently, Large High Altitude Air Shower Observatory (LHAASO) and Tibet air shower observations have identified a number of PeVatron candidates (Cao et al. 2021; Tibet ASγ Collaboration et al. 2021), which may include a few SNRs. These theoretical and observational developments suggest a cutoff energy in the range 10^5–10^6 GeV for SNRs. At the high-energy end, CRs above $\sim 10^9$ GeV are considered to have an extragalactic origin, possibly originating from galaxy clusters (Kang et al. 1996), radio galaxies (Rachen & Biermann 1993), active galactic nucleus jets (Mannheim et al. 2000), or gamma-ray bursts (Waxman 1995).

There is a gap between the contribution from SNRs and the extragalactic component, which lies in the range of $\sim 10^7$–10^9 GeV, the region between the so-called "knee" and "ankle" (also known as the "shin" region). To explain this gap in the all-particle CR spectrum, a few models have been proposed in the literature. Biermann & Cassinelli (1993) and Thoudam et al. (2016) have discussed the explosion of Wolf–Rayet stars embedded in the wind material from the same stars as a potential acceleration site of CRs in the range of $\sim 10^7$–10^9 GeV. However, there may be some problems with this scenario. A uniform distribution of Wolf–Rayet stars in the Galaxy was assumed, which is unrealistic. Moreover, there are many uncertainties in the crucial parameter of the magnetic field of the Wolf–Rayet stars. For a proton cutoff energy of 1.1×10^8 GeV, the surface magnetic field of a Wolf–Rayet star is required to be $\approx 10^4$ G in this model (Thoudam et al. 2016), while realistic predictions for the same are in the range of a few hundred gauss (Blazère et al. 2015; Neiner et al. 2015). Although no direct magnetic signature has been detected in any

of the Wolf–Rayet stars, using Bayesian statistics, Bagnulo et al. (2020) have estimated their surface magnetic fields to be of the order of a few kilogauss.

The idea of a Galactic wind termination shock (WTS) to accelerate high-energy CRs also has problems. The effect of Galactic winds on the transport of CRs in the Galaxy has been discussed in detail (Lerche & Schlickeiser 1982; Bloemen et al. 1993; Strong & Moskalenko 1998; Jones et al. 2001; Breitschwerdt et al. 2002). Following these developments, Jokipii & Morfill (1987), Zirakashvili & Völk (2006), and Thoudam et al. (2016) introduced these CRs originating from a Galactic WTS as a possible candidate for the "second" (between "knee" and "ankle") component of Galactic CRs. The CRs originating from the Galactic wind (GW-CRs) are believed to mostly contribute to the higher energy range. This is due to the increasing effect of advection over diffusion at lower energy, preventing particles from reaching the Galactic disk. Higher-energy particles, which diffuse relatively faster, can overcome the advection and reach the disk more effectively. Thoudam et al. (2016) have used a distance of $\sim$100 kpc for the Galactic WTS. Bustard et al. (2017) have argued that in order for the CRs to reach 10^8 GeV, either the outflow speed needs to be of order $\sim$1000 km s^{-1} or the magnetic field needs to be amplified. However, realistic simulations of outflows from Milky Way–type galaxies do not find signatures of such strong outflows/shocks. Sarkar et al. (2015) showed that the outer shock due to the Galactic wind weakens and continues to propagate as a sound wave through the circumgalactic medium. The termination shock remains confined within $\lesssim$tens of kiloparsecs and disappears after the mechanical power has stopped being injected. In addition, the observed nuclear abundances suggest lighter nuclei in contrast to the expectation from the Galactic wind model in the 10^7–10^9 GeV energy range. Thus, this model has been disfavored. In order to explain the observed all-particle spectrum in the range 10^7–10^9 GeV, an appropriate model of CRs is still required.

Coming back to the DSA mechanism of CR acceleration in SN shocks, this standard scenario is known to bear several ailing problems (e.g., Gabici et al. 2019). The acceleration scenario cannot explain some of the observed features of CRs, such as the excess of Ne^{22}/Ne^{20} in CRs compared to standard cosmic abundances in the interstellar medium (ISM; Wiedenbeck et al. 1999; Binns et al. 2008), proton acceleration up to a greater than PeV (10^6 GeV) energy range, and so on. Various additional CR acceleration sites are reported in the literature to solve these paradigms; young, massive star clusters are one of those other possible sources of CRs in our Galaxy (Knödlseder 2013; Bykov 2014; Aharonian et al. 2019). Recently, the γ-ray observations by LHAASO, HESS, Fermi-LAT, and HAWC have provided evidence of CR acceleration up to very high energy in a few massive star clusters like Westerlund 1 and Cygnus (Aharonian et al. 2019; Abeysekara et al. 2021). These star-forming regions have been discussed as potential candidates for CR accelerators (e.g., Bykov 2014); these γ-ray observations have strengthened the hypothesis of CR acceleration in these environments. Recently, Gupta et al. (2020) have shown that the excess ($^{22}Ne/^{20}Ne$) ratio can be explained by considering the WTS of massive star clusters as CR accelerators. Recently, Tatischeff et al. (2021) showed that the refractory elements of Galactic CRs are produced in superbubbles. This theoretical and observational evidence prods us to study the total contribution of CRs originating from the distribution of massive star clusters in our Galaxy.

Star clusters, which are the birthplace of massive stars (which ultimately explode as SNe), give rise to continuous mass outflow in the form of stellar wind. These are mainly located in dense molecular clouds and weigh of the order of several thousand solar masses (Longmore et al. 2014). Star clusters host both massive stars and SN explosions, which produce a low-density bubble around them (Weaver et al. 1977; Gupta et al. 2018). Young star clusters contain sufficient kinetic energy supplied by interacting stellar winds, which can accelerate protons up to $\sim 10^7$ GeV. Considering heavier nuclei, this CR component originating from star clusters can, therefore, be considered as the second component of Galactic CRs, which can explain the observed all-particle spectrum in the energy range of 10^7–10^9 GeV. Bhadra et al. (2022), using hydrodynamic simulations, showed that the observed distribution of γ-rays can be explained by invoking CR acceleration in the Westerlund 1 cluster.

Following the above discussion, it is clear that (1) Galactic SNe can accelerate particles up to a few times 10^6 GeV energy and (2) extragalactic components can explain the all-particle spectrum above $\sim 10^9$ GeV energy. The gap in the energy range cannot be explained using only these two components, and we require another Galactic component to explain the observed data in the range 10^7–10^9 GeV. Our main focus in this paper is the second component of Galactic CRs. In this regard, we propose CR contribution from the population of massive star clusters as a source of the observed all-particle CR spectrum in the range $\sim 10^7$–10^9 GeV. This may act as a bridge between the SNR component and the extragalactic component and fill the gap in the desired energy range.

We begin with some basics in Section 2. The details of our proposed model are described in Section 3. We present our results in Section 4 and compare our model with other models in Section 5. In Section 6, we consider various models for the extragalactic CR component. This is followed by further discussion in Section 7 and a conclusion in Section 8.

2. Existing Components of Cosmic Rays

2.1. First Galactic Component: SNR-CRs

As mentioned in the Introduction, SNRs are the most likely candidate for CR acceleration up to $\sim 10^6$ GeV energy (Lagage & Cesarsky 1983). The DSA at strong shocks produces a power-law spectrum with an index of approximately -2 (Krymskii 1977; Bell 1978; Blandford & Ostriker 1978; Caprioli et al. 2011). We have adopted the model of Thoudam et al. (2016) for the CR component from Galactic SNRs (SNR-CR component). After the acceleration in the strong shock of SNRs, CR particles escape the remnants and propagate through the ISM via diffusion. These CR particles can be reaccelerated repetitively by expanding SNR shock waves already existing in the ISM during their propagation. These shocks are mainly produced by older remnants and are relatively weak.

We use the same contribution of the SNR-CR component as presented in Thoudam et al. (2016). Their calculation assumes an exponential cutoff for the proton source spectrum at $E_c = 2.5 \times 10^6$ GeV. This value has been chosen by fitting the observed all-particle spectrum. The maximum energy of SNR-CRs corresponds to the cutoff energy of iron nuclei, which is $26 \times E_c = 6.5 \times 10^7$ GeV. This result shows that

SNR-CRs can contribute only ∼30% of the total observed intensity above $\sim 2 \times 10^7$ GeV (Thoudam et al. 2016). Therefore, additional components are required to explain the all-particle spectrum in the $\gtrsim 10^7$ GeV range.

2.2. Extragalactic Component

Various previous works have already pointed out that the "ankle"-like feature of the CR spectrum at $\gtrsim 10^9$ GeV can be explained if we consider the propagation effects of the extragalactic component (mainly proton) in the evolving microwave background (Hillas 1967; Berezinskii & Grigor'eva 1988; Berezinsky et al. 2006; Aloisio et al. 2012, 2014). We consider two different models for the extragalactic component: the "UFA model" (Unger et al. 2015), and a combination of the minimal (di Matteo 2015) and primordial cluster shock (PCS) models (Rachen 2015; Thoudam et al. 2016). We refer to this combined model as the "MPCS model."

Unger et al. (2015) consider acceleration of energetic nuclei at the shocks associated with gamma-ray bursts or tidal disruption events and photodisintegration of these particles in the photon background present inside the source region. In this model, only the highest-energy particles having an escape time shorter than the photodisintegration time can escape the source region, leading to a strong proton component in the energy region below the ankle. We call this the "UFA model" of the extragalactic component. In addition to the all-particle CR spectrum, data of the primary composition in the ultrahigh energy range have become available in the past few years.

The "minimal model" has been derived from CR composition measured by the Pierre Auger Observatory (di Matteo 2015) and assumes uniformly distributed sources in a comoving volume that produce a power-law CR spectrum with some cutoff at a particular rigidity R_c (rigidity is defined as Apc/Ze, where A/Z is nuclear mass/charge, p is momentum, e is the charge of the electron, and c is the speed of light in vacuum). Above $\sim 3 \times 10^{10}$ GeV, the spectrum exhibits a steep cutoff that is mainly due to the intrinsic cutoff in the injection spectrum (di Matteo 2015), and not due to the GZK absorption (Greisen 1966; Zatsepin & Kuz'min 1966) during the propagation.

The PCS model is based on the universal scaling argument. It takes into account the acceleration of primordial proton and helium mixture by PSCs, which are mainly the accretion shocks expected from clusters of galaxies during the structure formation. In this scenario, the acceleration of CR particles is limited by losses due to pair production in the cosmic microwave background. This component is not expected to reach ultrahigh energies. Consequently, the minimal model plus the "primordial cluster component" was introduced by Rachen (2015), where the acceleration of heavy nuclei at shocks of gamma-ray bursts or in tidal disruption events is considered.

3. Second Galactic Component: Cosmic Rays from Star Clusters

The all-particle CR spectrum has two main features: a steepening of the spectral index from −2.7 to −3.1 at about 3 PeV, commonly known as the "knee," and a flattening back to −2.7 at about 4×10^9 GeV, generally known as the "ankle." Therefore, we need to assume a cutoff in the Galactic component immediately below the "ankle" to explain the observed spectrum. This is a "second knee" feature in the CR spectrum. For a typical magnetic field of 3 μG in the Galaxy, CRs with energy $Z \times 10^8$ GeV have a Larmor radius of $36/Z$ pc, which is much smaller than the extent of the diffusion halo of the Galaxy. This implies that CRs with the energy around the second knee remain confined within the Galaxy. This also suggests that the observed cutoff at this energy is due to some CR accelerators different from SNRs, as the latter accelerate particles only up to a few $\times 10^6$ GeV.

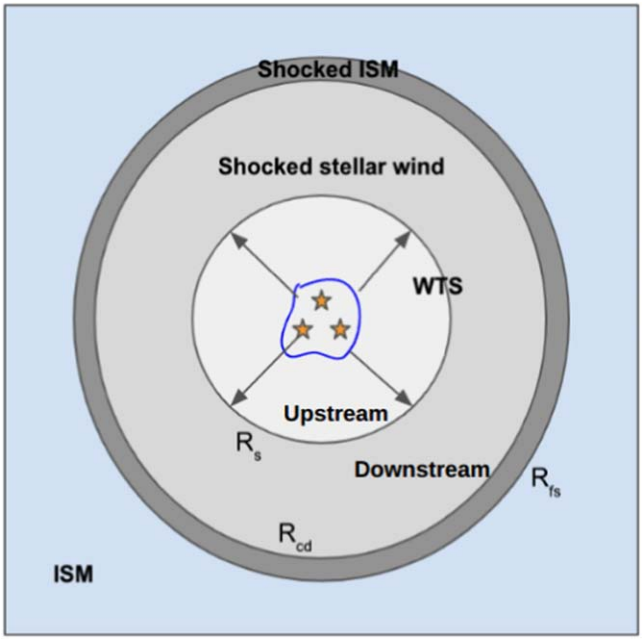

Figure 1. Schematic diagram of a stellar wind bubble. The position of termination shock is R_s; R_{cd} and R_{fs} are contact discontinuity and forward shock positions, respectively.

In the following, we discuss one potential scenario of another Galactic component of CRs: the acceleration of CRs by the young, massive star clusters, which we briefly mentioned in Section 1. It has especially been speculated that the winds of massive stars may be a suitable location for the acceleration of CRs (Cesarsky & Montmerle 1983; Webb et al. 1985; Gupta et al. 2018; Bykov et al. 2020). CRs can be accelerated in the fast stellar wind of star clusters, and in particular, two scenarios can be important: (1) CR acceleration in the WTS (Gupta et al. 2018) and (2) acceleration by SN shocks embedded in the stellar winds (Vieu et al. 2022). Those CRs accelerated in young star clusters with age $\leqslant 10$ Myr can contribute significantly to the observed total flux of CRs (Gupta et al. 2020). Recently, LHAASO has observed γ-rays in the PeV energy range from young, massive star clusters (Cao et al. 2021), which can be associated with CR acceleration in those clusters.

Figure 1 shows a schematic diagram of a stellar wind bubble around a compact star cluster. There are several distinct regions inside the bubble, such as (a) the free wind region, where the stellar wind originating from the source expands adiabatically; (b) the WTS; (c) the shocked wind region containing slightly denser gas; and (d) the outermost dense shell containing the swept-up ambient gas. CRs can be accelerated in the central region, as well as in the shocks of the cluster. After getting accelerated to very high energy, CRs will diffuse outward from the source into the ISM.

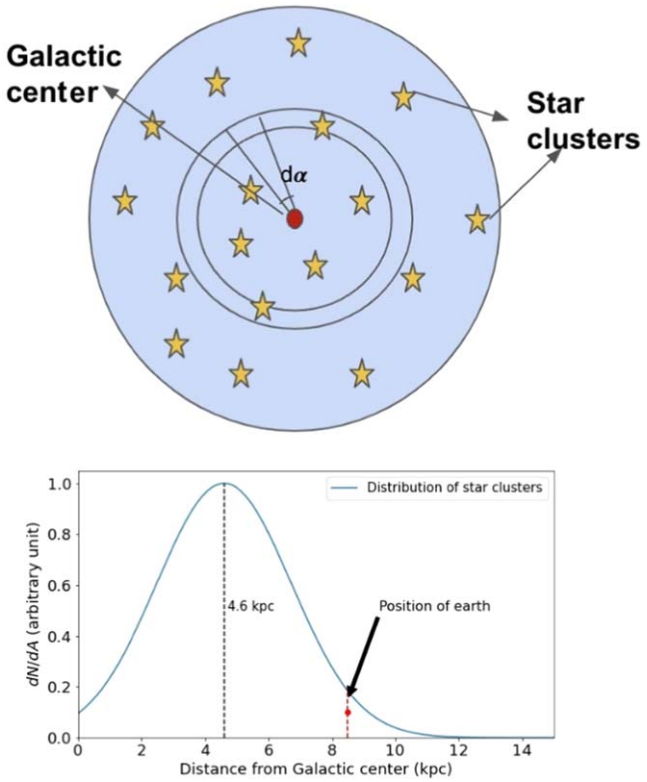

Figure 2. Top: schematic distribution of star clusters in the Galactic plane (face-on view); each star indicates a star cluster on the plane. Bottom: the surface density (number per area) of star clusters (Σ; see Equation (2)) as a function of distance from the Galactic center.

3.1. Distribution of Star Clusters in the Galactic Plane

Star clusters are distributed all over the Galactic plane (shown in Figure 2), and each star cluster creates a superbubble-like structure around itself (Weaver et al. 1977; Gupta et al. 2018). Bronfman et al. (2000) observed 748 OB associations across the Galactic disk and found their distribution (see Figure 2) to peak at $R_p = 0.55R_0$, ($R_0 = 8.5$ kpc is the solar distance from the Galactic center). We find that their inferred (differential) star cluster distribution can be roughly fitted by

$$dN_c(r) = \Sigma_0\, e^{\frac{-(r-R_p)^2}{\sigma^2}}\, 2\pi r\, dr, \tag{1}$$

where r is the Galactocentric distance, $\sigma = 3$ kpc, and Σ_0 is the normalization constant in units of kpc^{-2}. This denotes the number of star clusters in an annular ring of radius r to $r + dr$. The surface density of the clusters can be obtained by dividing this number by the surface area of the annular ring ($2\pi r\, dr$), as

$$\nu(r) = \Sigma_0\, e^{\frac{(-r-R_p)^2}{\sigma^2}}, \tag{2}$$

where $\Sigma_0 \sim 14$ kpc^{-2} (Nath & Eichler 2020). We have used a minimum number of 10 and a maximum number of 1000 OB stars in a cluster (these are somewhat arbitrary, and we later discuss the impact of these choices).

3.2. Transport of CRs Originating from Star Clusters in the Galaxy

After getting accelerated in SNR and star cluster shocks, CRs propagate through the Galaxy. This propagation is mainly dominated by diffusion and energy loss due to interaction with ISM material. Some fraction of the propagating CRs can be reaccelerated up to higher energy by the interaction with existing weaker shocks that have been generated from older SNRs in the ISM. This process has been discussed in detail in Thoudam & Hörandel (2014). The transport equation for CR nuclei in a steady state can be written as

$$\nabla \cdot (D\nabla N) - [nv\sigma + \zeta]\delta(z)N + \left[\zeta sp^{-s}\int_{p_0}^{p} du\, N(u)u^{s-1}\right]\delta(z) = -Q(r, p)\delta(z). \tag{3}$$

Here we include spatial diffusion (first term on the left-hand side), reacceleration (terms with coefficient ζ), and interaction losses ($\propto\sigma$, the loss cross section) of the CR particles, as mentioned above. The diffusion coefficient $D(p)$ depends on the momentum of CR particles. Here n represents the averaged surface density (number density per unit area) of interstellar atoms in the Galaxy, $v(p)$ is the CR particle velocity, $\sigma(p)$ is the cross section of inelastic collision, N is the differential number density (number per unit volume per momentum), and ζ is the rate of reacceleration. The third term involving the momentum integral represents the generation of higher-energy particles via the reacceleration of lower-energy particles. It has been assumed that a CR population is instantaneously reaccelerated to form a power-law distribution with an index of $s \sim 4.5$ (Thoudam & Hörandel 2014). We consider a cylindrical geometry for the diffusion halo denoted by the radial coordinate r and vertical direction z. The diffusive halo has upper and lower boundaries at $z = \pm H$ and a radial boundary at 20 kpc. A significant fraction of CRs that reach Earth is produced from those sources located within a distance $\sim$5 kpc (Taillet & Maurin 2003).

The term on the right-hand side, $Q(r, p)\delta(z)$, represents the injection rate of CRs per unit volume in the momentum bin $[p, p + dp]$ by the sources. The $\delta(z)$ term denotes that all sources are confined to the Galactic plane $z = 0$. Similarly, reacceleration and loss regions are confined within the Galactic midplane.

The injection term $Q(r, p)$ can be written as a combination of a space-dependent part and a momentum-dependent part, i.e.,

$$Q(r, p) = \nu(r)H[R - r]\, H[p - p_0]\, Q(p),$$

where $\nu(r)$ (see Equation (2)) represents the number of star clusters per unit surface area on the Galactic disk (see Section 3.1 for details), $H[t] = 1(0)$ for $t > 0(< 0)$ is the Heaviside step function, and p_0 (which is the lower limit in the integral in Equation (3)) is the low-momentum cutoff introduced to approximate the ionization losses. Wandel et al. (1987) showed that the ionization effects could be taken into account if we truncate the particle distribution below $\sim$100 MeV nucleon^{-1}. In our calculation, we introduce a low-energy cutoff of 100 MeV nucleon^{-1}. Our assumed distribution of star clusters, motivated by observations, has a peak at $\sim$4.6 kpc ($0.55R_0$, where R_0 is the distance of Earth from the Galactic center $\sim$8.5 kpc) and then decreases rapidly at large distances (for details see Section 3.2).

The expression for surface density of star clusters ν has been calculated in Section 3.1, and the power-law source spectrum is described in Section 3.3. The energy-dependent diffusion

coefficient as a function of particle rigidity follows

$$D(\rho) = D_0\,\beta(\rho/\rho_0)^{\delta},$$

where D_0 is the diffusion constant; $\rho = Apc/Ze$ is the particle rigidity; $\beta = v(p)/c$, with $v(p)$ the CR particle velocity and c the speed of light; $\delta = 0.33$ is the diffusion index; and $\rho_0 = 3$ GV is a normalization constant.

In this injection–diffusion–reacceleration[4] model, the rate of reacceleration depends on the rate of SN explosions and the fractional volume occupied by SNRs in the Galaxy. The reacceleration parameter ζ can be expressed as $\zeta = \eta V \nu_{\rm SN}$, where $V = 4\pi\mathfrak{R}^3/3$ is the volume occupied by each SNR of radius $\mathfrak{R}$ reaccelerating the CRs. Here η is a correction factor that takes care of the actual unknown size of the remnants, and $\nu_{\rm SN}$ is the rate of SN explosions per unit surface area in the Galactic disk. The values of $\mathfrak{R}$ and $\nu_{\rm SN}$ have been taken as 100 pc and 25 SNe $\rm Myr^{-1}\,kpc^{-2}$, respectively (Thoudam & Hörandel 2014).

The solution of Equation (3) can be obtained by invoking the Green's function method, considering the two separate transport equations for the regions below and above the Galactic disk ($z < 0$ and $z > 0$, respectively), and connecting the two solutions at the Galactic plane, i.e., $z = 0$, via a jump condition. Following this procedure, one can get Green's function $G(r, r', z, p, p')$ (Equation (A.20) of Thoudam & Hörandel 2014). After convolving the obtained Green's function with the assumed source distribution and integrating it over the Galactic plane, one can get the final solution (see Equation (6) of the same paper) for the CR density $N(r, z, p)$. Following the procedure described in Thoudam & Hörandel (2014), we get the solution of the transport Equation (3) as

$$N(r, z, p) = 2\pi \int_0^{\infty} dp' \int_0^{\infty} r' dr'\, G(r, r', z, p, p')Q(r', p').$$

Substituting the obtained $G(r, r', z, p, p')$ (Thoudam & Hörandel 2014) and the assumed source distribution in the above equation, the CR density at Earth ($r = 8.5$ kpc) can be calculated by evaluating the above solution at $z = 0$ since our solar system lies close to the Galactic plane. More explicitly, the differential number density measured at the location of Earth is

$$\begin{aligned} N(r, p) = &\int_{r'=0}^{R} \int_{k=0}^{\infty} \Sigma_0 \frac{J_0[k(r - r')]}{L(p)}\, k\, dk\, e^{\frac{-(r'-R_p)^2}{\sigma^2}}\, r'\, dr' \\ &\times \left[Q(p) + \zeta s p^{-s} \int_{p_0}^{p} p'^{s}\, dp'\, Q(p')A(p') \right) \\ &\times \left(\exp\left(\zeta s \int_{p'}^{p} A(u)du \right) \right], \end{aligned} \tag{4}$$

where $R = 20$ kpc is the radial boundary of the Galaxy, Σ_0 is the number density of star clusters, J_0 is the Bessel function of order zero, and the functions $A(p)$ and $L(p)$ are given by (see Thoudam & Hörandel 2014 for details)

$$L(p) = 2D(\rho)k\,\coth(kH) + nv\sigma(p) + \zeta, \tag{5}$$

$$A(p) = \frac{1}{pL(P)}. \tag{6}$$

Equation (4) gives the differential number density, i.e., number per unit volume per unit momentum of CR particles measured at Earth. All the necessary terms needed to solve Equation (4) are discussed in Sections 3.2–3.5.

3.3. Injection Spectra of Cosmic-Ray Nuclei

The CR source spectrum $Q(p)$ from star clusters is assumed to follow a power law in total momentum Ap with an exponential cutoff, where A is the mass number of the nucleus. We write the differential number of CR particles with nucleon number A, having momentum per nucleon in the range (p, $p + dp$), as

$$Q(p) = Q_0(Ap)^{-q} \exp\left(-\frac{Ap}{Zp_{\rm max}} \right). \tag{7}$$

Here Q_0 is a normalization constant that is proportional to the fraction of total wind kinetic energy f channeled into CRs by a single star cluster. We call this the "injection fraction," which is a free parameter and can be estimated by comparing the model result with observations. In addition, q is the spectral index, $p_{\rm max}$ is the cutoff momentum (for a single nucleon), and Ap is the total momentum of a particle with the mass number A and the atomic number Z.

3.4. Maximum Energy Estimate of Accelerated Particles

For the estimation of the maximum accelerated energy of CR particles, we consider two different acceleration scenarios inside a young star cluster: acceleration at a WTS, and acceleration of particles around an SNR shock inside a star cluster.

3.4.1. Acceleration at Wind Termination Shock

In Equation (7), $p_{\rm max}$, which represents the maximum momentum of accelerated CRs, depends on the extension of the accelerating region for a stellar wind bubble of the cluster. Typically, this accelerating region can be taken as the distance to the WTS ($R_{\rm WTS}$) from the center of the cluster. The maximum energy is achieved when the diffusion length becomes comparable to the size of the shock (in this case the WTS), for beyond this limit the particles escape out of the accelerating region. In the case of Bohm diffusion, $\kappa = pc^2/(\zeta qB)$, the maximum energy is then (Vieu et al. 2022)

$$E_{\rm max} \sim \zeta\, q\, B_{\rm WTS}\, R_{\rm WTS}\, \frac{V_w}{c}. \tag{8}$$

Here $R_{\rm WTS}$ is the radius of the WTS. In the above equation, V_w is the velocity of stellar wind, $B_{\rm WTS}$ is the value of the magnetic field at the WTS position, and $\zeta = 3r_g/\lambda$, with λ the mean free path due to the magnetic field. The Bohm diffusion, which is the most optimistic scenario, corresponds to the limit $\zeta = 3$.

[4] For typical parameters, reacceleration only affects the CR spectrum below 10^5 GeV (Thoudam & Hörandel 2014) and so is irrelevant for the energy range considered in this work.

We follow the arguments advocated by Vieu et al. (2022) to estimate the magnetic field in the cluster core,

$$B_c \sim 150\left(\frac{n_c}{10\ \mathrm{cm}^{-3}}\right)^{1/6}\left(\frac{\eta_T}{0.1}\right)^{1/3}\left(\frac{N_{\mathrm{OB}}}{100}\right)^{2/9} \times \left(\frac{R_c}{1\mathrm{pc}}\right)^{-2/3} \mu\mathrm{G}. \quad (9)$$

Here n_c is the core density, η_T is the efficiency of generation of turbulence, N_{OB} is the number of OB stars in the cluster, and R_c is the core radius of the cluster. The magnetic field advected into the free wind region has a $1/r$ radial profile. Therefore, the magnetic field at the position of the WTS and cluster core can be related using $B_c R_c = B_{\mathrm{WTS}} R_{\mathrm{WTS}}$. Therefore, Equation (8) can be expressed as

$$E_{\max} \sim \zeta\ q\ B_c\ R_c\ \frac{V_w}{c}. \quad (10)$$

This leads to a maximum estimate:

$$E_{\max} \sim 6\left(\frac{\zeta}{3}\right)\left(\frac{n_c}{10\ \mathrm{cm}^{-3}}\right)^{1/6}\left(\frac{\eta_T}{0.2}\right)^{1/3}\left(\frac{N_{\mathrm{OB}}}{1000}\right)^{2/9} \times \left(\frac{R_c}{1\ \mathrm{pc}}\right)^{1/3}\left(\frac{v_w}{2000\ \mathrm{km\ s}^{-1}}\right)\mathrm{PeV}. \quad (11)$$

Equation (11) gives a conservative estimate of $E_{\max} = 6\ PeV$ (6×10^6 GeV) for the maximum attainable energy of protons. Note that this value is a few times higher than the maximum accelerated energy for the SNR-CR scenario.

However, in the realistic scenario, the magnetic field may be amplified in the accelerating region owing to the existence of turbulence and to instabilities driven by CR streaming in the upstream region of the WTS, which can therefore increase the estimated value of maximum accelerated energy. There are other uncertainties as well (e.g., in η_T, wind velocity v_w) that can conceivably increase the maximum energy by a factor of a few.

3.4.2. Acceleration at SNR Shock inside Star Clusters

Another potential scenario for CR acceleration inside the young star cluster is the SNR shocks propagating in the free wind region of the cluster. Particles will be accelerated during the expansion of the SNR shock upstream of the WTS. This idea has been studied extensively by Vieu et al. (2022), and the maximum energy has been estimated by the authors as follows:

$$E_{\max} \sim 21\left(\frac{V_c}{5000\ \mathrm{km\ s}^{-1}}\right)\left(\frac{\zeta}{3}\right)\left(\frac{R_c}{1\ \mathrm{pc}}\right)\left(\frac{N_{\mathrm{OB}}}{1000}\right)^{2/9} \times \left(\frac{n_c}{10\ \mathrm{cm}^{-3}}\right)^{1/6}\left(\frac{\eta_T}{0.2}\right)^{1/3}\left[1-\left(\frac{R_c}{R_{\mathrm{WTS}}}\right)^{1/7}\right]\mathrm{PeV}. \quad (12)$$

For a typical young cluster $R_{\mathrm{WTS}}/R_c \sim 5-30$, which gives $(1-(R_c/R_{\mathrm{WTS}})^{1/7}) \sim 0.2$–$0.4$ (Vieu et al. 2022). This estimate can give a maximum energy of a few PeV for protons. However, if an SN launches a very fast shock in the free wind region of a compact cluster with velocity $\geqslant 2 \times 10^4$ km s^{-1}, it can accelerate protons up to a few tens of PeV energy. Note that this high velocity of SNR shock inside a clumpy star cluster may efficiently drive MHD turbulence to generate a high value of the magnetic field, which will likely result in a higher value of maximum energy.

The recent detection of γ-rays above PeV by LHAASO from some sources indeed indicates that these sources can accelerate particles up to at least a few tens of PeV because, at high energy, the γ-ray energy can be approximated as $E_{\mathrm{cr}} \approx 10E_\gamma$. Some of those sources possibly are young, massive clusters (see extended Table 2 of Cao et al. 2021). The γ-ray photons from the LHAASO J2032 + 4102 source have the highest energy of 1.4 PeV, which corresponds to tens of PeV for CR protons.

3.5. Elemental Abundances in Star Cluster Winds

We consider a simple stellar population formed at time $t = 0$ with an initial mass function $\frac{dn}{dm} \propto m^{-2.35}$ (Salpeter 1955). We can calculate the elemental abundances in the wind material following the procedure described in Roy et al. (2021). Now,

$$M_w(X, m, t) = \int_0^t \dot{m}_w(X, m, t')dt' \quad (13)$$

is the cumulative mass of element X ejected in winds by a star of initial mass m up to age t, where

$$\dot{m}_w(X, m, t') = \mathrm{mass\ \ fraction}(X, m, t') \times \dot{m}(m, t') = f(X, m, t') \times \frac{dm_{\mathrm{star}}}{dt'}. \quad (14)$$

We use the mass-loss rate for each nucleus $\dot{m}(X, m, t')$ using models for nucleosynthesis in massive stars and their return to the ISM via winds (A. Roy 2023, private communication). Hence, the elemental abundance of a particular element X can be calculated using

$$f(X, m) = \frac{M_w(X, m, t)}{M_{w,\mathrm{tot}}(m, t)} = \frac{\int_0^t \dot{m}_w(X, m, t')dt'}{\int_0^t \dot{m}(m, t')dt'}. \quad (15)$$

We have taken into account evolution until the core carbon burning time, which implies the maximum time of the evolution of a star with mass m as the upper limit of the integration. The mass-weighted elemental abundance of element X can be calculated using the following expression invoking the Salpeter mass function:

$$\langle f(X)\rangle = \frac{\int_0^m f(X, m)Am^{-2.35}dm}{\int_0^m Am^{-2.35}dm}. \quad (16)$$

Using this method, we have calculated the mass-weighted mean individual elemental abundance in the ejected stellar wind material. We have used the results of a state-of-the-art evolutionary model. The elemental abundances have been calculated considering the rotation-driven instabilities inside the star, the correct abundances of elements, and the mass-loss rate from the stellar surface.

3.6. Average Kinetic Luminosity of Clusters

Our assumption requires a certain fraction of the total wind kinetic energy to go into CRs. Therefore, we need the value of the average kinetic luminosity of a cluster using a distribution of OB associations over the luminosity range. Oey & Clarke (1997) assume that the mechanical luminosity function of the OB association is given by $\phi(L) \propto L^{-2}$. We use this distribution to calculate the average luminosity of clusters with kinetic

Table 1
Source Spectral Indices q and Fractional Abundances of Different Elements in the Wind Material

Elements	q	Fractional Abundances in Winds
Proton	2.25	0.86
Helium	2.23	0.13
Carbon	2.20	3.32×10^{-3}
Oxygen	2.24	8.51×10^{-4}
Neon	2.24	8.83×10^{-5}
Magnesium	2.28	3.62×10^{-5}
Silicon	2.24	3.42×10^{-5}
Iron	2.24	3.72×10^{-5}

Note. The elemental abundances are calculated following Roy et al. (2021).

luminosity in the range $L_{\rm min} = 10^{37}$ erg s^{-1} (corresponds to $N_{\rm OB} = 10$) to $L_{\rm max} = 10^{39}$ erg s^{-1} (corresponds to $N_{\rm OB} = 1000$) as follows:

$$\langle L_w \rangle = \frac{\int_{L_{\rm min}}^{L_{\rm max}} \phi(L) L \, dL}{\int_{L_{\rm min}}^{L_{\rm max}} \phi(L) dL} \sim 4.5 \times 10^{37} \text{ erg s}^{-1}. \quad (17)$$

Note that we adopt a minimum number of 10 OB stars for the production of CRs, and the largest OB association in our Galaxy has 1000 OB stars. The dependence of $\langle L_w \rangle$ on $L_{\rm max}$ is weak, but there is a sensitive dependence on $L_{\rm min}$, the implications of which we discuss later.

4. Model Prediction for the Second Component of Galactic Cosmic Rays

The values of CR propagation parameters (D_0, δ; the normalization of the diffusion coefficient and its power-law dependence on momentum) and reacceleration parameters (η, s; the SNR filling factor and reacceleration power-law index) have been calculated by comparing the observed ratio of boron to carbon abundance with the value obtained by the adopted model. The best-fit values are $D_0 = 9 \times 10^{28}$ cm^2 s^{-1}, $\eta = 1.02$, $s = 4.5$, and $\delta = 0.33$ (Thoudam & Hörandel 2014). We have also used these values in our model. For the interstellar matter density (n), the averaged density in the Galactic disk within a radius equal to the size of the diffusion halo H was considered. We choose $H = 5$ kpc (Thoudam et al. 2016), which gives an averaged surface density of atomic hydrogen of $n = 7.24 \times 10^{20}$ atoms cm^{-2} (Thoudam & Hörandel 2014). To account for the helium abundance in the ISM, we add an extra 10% to n. The radial extent of the source distribution is taken as $R = 20$ kpc. The inelastic cross section for protons ($\sigma(p)$) is taken from Kelner et al. (2006).

Since we are interested in the acceleration of CRs in the WTS, as well as around SNR shocks inside the free wind region of the star cluster, the relevant abundances correspond to those in the stellar wind for massive stars. For this purpose, we use the stellar wind abundances for massive stars beginning with the zero-age main-sequence (ZAMS) phase. We have used the surface abundance of massive stars as a function of time, calculated after properly taking into account the effect of stellar rotation. The spectral indices for different elements are given in Table 1. Note that these values are slightly different from the spectral indices assumed in Thoudam et al. (2016) for the SNR-CR component. In addition, the stellar wind elemental abundances are mentioned in Table 1, which are calculated using the method described in Roy et al. (2021; provided to us by A. Roy 2023, private communication). We have then averaged the abundances over time and mass distribution of stars in the cluster, as described in Section 3.5. Using these values of various parameters, we calculate the particle spectra for different CR elements (proton, helium, carbon, oxygen, neon, magnesium, silicon, and iron). The CR spectral indices (q) of source spectra for the individual elements are very similar to each other and are chosen to match the observed individual nuclear abundances in CRs closely.

Figure 3 shows the star cluster contribution to CRs using different parameters mentioned earlier. We have used the maximum energy for the proton as 5×10^7 GeV (50 PeV) and the injection fraction of ∼5%. These values of the parameters are chosen to match the observed spectra with our theoretical model. It is important to mention that in Section 3.4 we have estimated the maximum accelerated energy considering different scenarios in a star cluster. The maximum energy can go up to a few tens of PeV (especially for the SNR shock inside the star cluster scenario), although our used value is admittedly on the higher side. In addition, recently Vieu & Reville (2023) have shown that the SNR shocks inside a star cluster scenario can explain the all-particle CR spectrum in the region between "knee" and "ankle." Therefore, star clusters are likely a possible candidate for CR acceleration between a few times 10^6 and 10^9 GeV.

In addition, if one uses a higher lower limit of $N_{\rm OB} = 30$ instead of 10, then the injection fraction will need to be increased to match the observed spectrum. The data points correspond to different measurements. For lower energy ranges, the individual spectra are fitted to the observed elemental spectra. We consider eight elements (proton, helium, carbon, oxygen, neon, magnesium, silicon, and iron) for our calculations, and the total contribution (solid brown curve in the Figure 3) is a combination of these eight elements.

5. All-particle Spectrum of Cosmic Rays

Figure 4 combines all three CR components to get the total all-particle spectrum of CRs and compares it with various observations. The SNR-CR component shown in this figure is calculated following the procedure mentioned in Thoudam et al. (2016), assuming a uniform distribution of SNRs in the Galactic plane and a proton spectrum cutoff of $\sim 2.5 \times 10^6$ GeV. For the extragalactic component, we have adopted the UFA model (Unger et al. 2015), which considers a significant contribution of extragalactic CRs below the ankle to reproduce the observed CR energy spectrum, as well as $X_{\rm max}$ (the depth of the shower maximum) and the variance of $X_{\rm max}$ above the ankle observed at the Pierre Auger Observatory (di Matteo 2015). With these two models (SNR and extragalactic), we have combined our proposed star cluster model with a proton spectrum cutoff at 5×10^7 GeV.

The total contributions from all three components can explain the observed features in the all-particle spectrum. In addition, the spectra of the individual elements can be explained well with the model. The flux of different elements has been measured well in the lower-energy region, but in the higher energy range, i.e., above 10^5–10^6 GeV, the observation data for individual elements are not available. Observed data points for all-particle CR spectra have been taken from various experiments like TIBET III (Amenomori et al. 2008), IceTop (Aartsen et al. 2013), Auger (The Pierre Auger Collaboration et al. 2013), and HiRes II (High Resolution Fly'S Eye Collaboration et al. 2009).

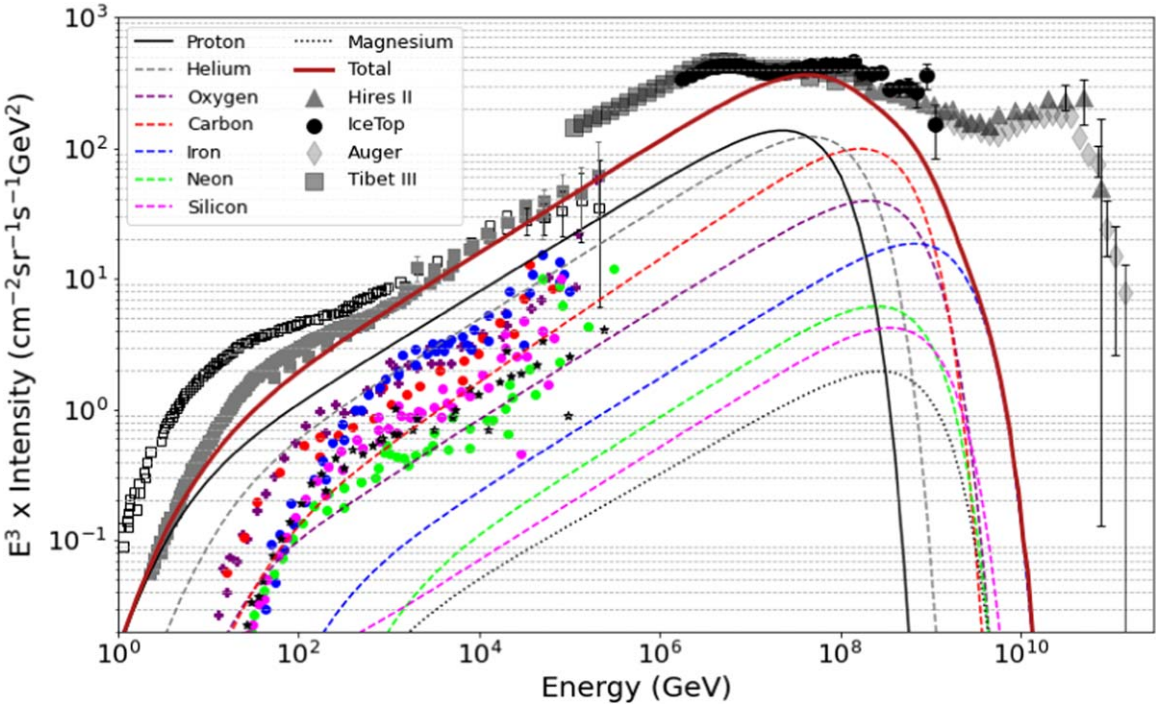

Figure 3. Model prediction for the star cluster model as a second galactic component considering an injection fraction ∼5%. The thick solid maroon line represents the total contribution from Galactic star clusters. Thin dashed lines represent the flux of individual elements. For the CRs generated from star clusters, an exponential energy cutoff for protons at $E_c = 5 \times 10^7$ GeV (50 PeV) is assumed. High-energy data: IceTop (Aartsen et al. 2013), Tibet III (Amenomori et al. 2008), the Pierre Auger Observatory (The Pierre Auger Collaboration et al. 2013), and HiRes II (High Resolution Fly'S Eye Collaboration et al. 2009). Low-energy data have been taken from CREAM (Ahn et al. 2009; Yoon et al. 2011), ATIC-2 (Panov et al. 2007), AMS-02 (Aguilar et al. 2015), PAMELA (Adriani et al. 2011), CRN (Mueller et al. 1991), HEAO (Engelmann et al. 1990), TRACER (Obermeier et al. 2011), KASCADE (Antoni et al. 2005), and DAMPE (An et al. 2019). We have only shown the high-energy data points with different symbols in the figure. Low data points: proton (black square), helium (gray square), oxygen (purple solid plus sign), carbon (red circle), iron (blue circle), neon (green circle), silicon (magenta circle), magnesium (black stars). The lower-energy data from various experiments are represented together by one symbol. The error bars for protons and helium have been shown, and the rest are not shown in the figure.

Several ground-based experiments, such as KASCADE, TUNKA, LOFAR, and the Pierre Auger Observatory, have provided measurements of the composition of CRs at energies above $\sim 10^6$ GeV. Heavier nuclei interact at a higher altitude in the atmosphere, which results in smaller values of $X_{\rm max}$ as compared to lighter nuclei. For comparison with the theoretical predictions, $\langle \ln A \rangle$, the mean logarithmic mass of the measured CRs, is of utmost importance. This can be obtained from the measured $X_{\rm max}$ values using the following relation mentioned in Hörandel (2003):

$$\ln A_i = \left(\frac{X^i_{\rm max} - X^{\rm p}_{\rm max}}{X^{\rm Fe}_{\rm max} - X^{\rm p}_{\rm max}} \right) \times \ln A_{\rm Fe}. \quad (18)$$

Here $X^{\rm p}_{\rm max}$ and $X^{\rm Fe}_{\rm max}$ represent the average maximum depths of the shower for protons and iron nuclei, respectively, and $A_{\rm Fe}$ is the mass number of iron nuclei. In Figure 5, we have also shown the obtained mean logarithmic mass using our model and compared it with the observational data.

We calculate the mean mass in the following way:

$$\langle \ln A \rangle = \frac{\sum_i \ln A_i \times {\rm Flux}_i}{\sum_i {\rm Flux}_i}, \quad (19)$$

where A_i denotes the mass number of an element i (we have considered eight elements: proton, helium, carbon, oxygen, neon, magnesium, silicon, and iron) and ${\rm Flux}_i$ is the obtained flux of element i using our model. Figure 5 shows that the results obtained using our star cluster model (green curve) follow the observed trend for the mean logarithmic mass in the total energy range from 10^8 to 10^{11} GeV when combined with the UFA model for the extragalactic CRs. In the energy range from about 2×10^7 GeV to 10^8 GeV, our prediction shows some deviation from the observed trend but still lies within limits presented in Kampert & Unger (2012).

To reiterate, the primary focus of this work has been to present a model incorporating stellar wind shocks that can explain the observed all-particle CR spectrum, especially in the energy range between 10^7 and 10^9 GeV. The discussion so far shows that we can indeed explain the observed data in this energy range using a CR component originating from massive star clusters. The required CR injection fraction for this component of ∼5% and an energy cutoff of $5 \times 10^7 Z$ GeV, as suggested by the fitting of the all-particle CR spectrum with our proposed stellar wind model, are entirely reasonable and therefore lend support to the idea that CRs from massive star clusters can fill the CR spectrum gap between the "knee" and the "ankle." We will discuss the implications of our result in Section 7. Before that, we discuss the dependence of the required injection fraction and cutoff energy on the chosen extragalactic component in Section 6 below.

6. Varying the Extragalactic Component

As mentioned in Section 2.2, we consider two different models of extragalactic CRs: the UFA model (Unger et al. 2015) and a combination of the PCS and minimal model (MPCS model; Rachen 2015; Thoudam et al. 2016). Depending on the chosen extragalactic component, the values of injection fraction and maximum cutoff energy can slightly

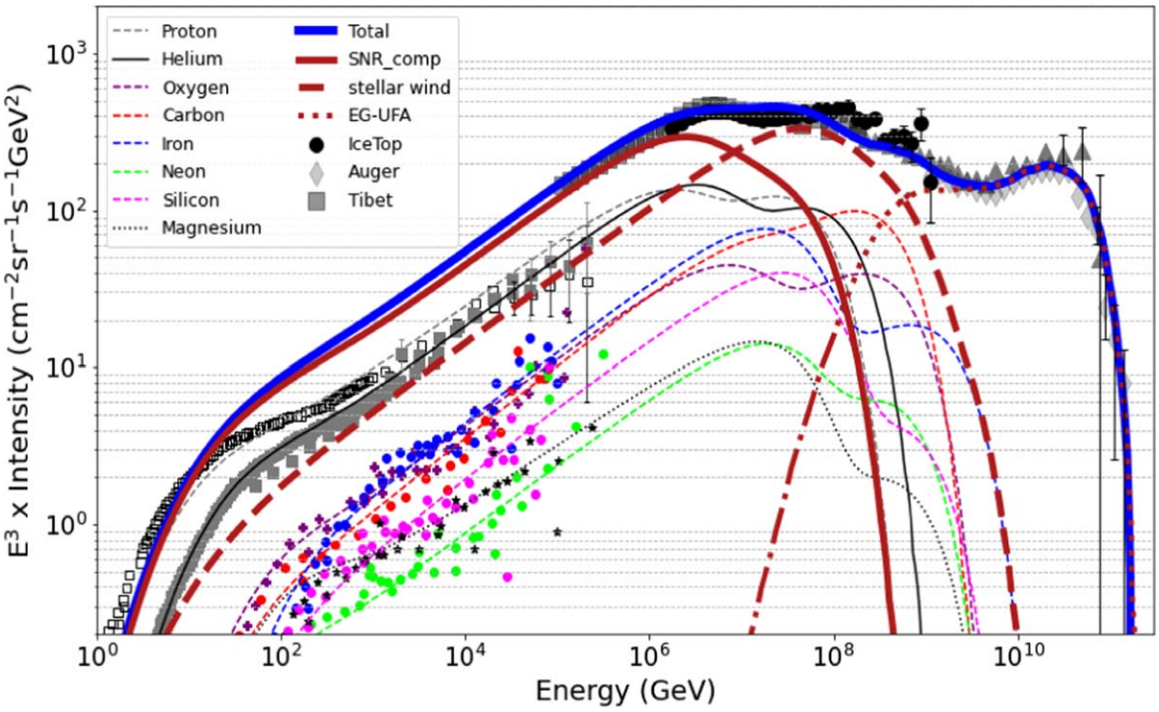

Figure 4. Model prediction for the all-particle spectrum using the Galactic star cluster CR model as the second galactic component. For the star cluster component, the considered injection fraction is ∼5% and the cutoff is at $5 \times 10^7 Z$ GeV. The thick dashed maroon line represents the total SNR-CRs, the thick solid maroon line represents star cluster CRs, the thick maroon dotted line represents the UFA model of the extragalactic CR component (EG-UFA) taken from Unger et al. (2015), and the thick solid blue line represents the total all-particle spectrum. The thin lines represent the total spectra for the individual elements, i.e., a combination of both SNR-CR and the CRs originating from star clusters. The figure shows the E^3 times the CR flux $I(E) = (c/4\pi)N(E)$ at the position of Earth measured by different experiments as a function of CR energy, where $N(E)$ is the differential number density of CR particles. High- and low-energy data are the same as in Figure 3.

change. The UFA and MPCS models predict a significant contribution of extragalactic CRs below the "ankle." All these different extragalactic models can explain the observations when combined with the SNR-CR component and the CR component from star clusters, although the UFA model somehow shows a smooth transition (Figure 4) between the Galactic and extragalactic components. The sharp increase near 10^9 GeV in the MPCS model (top panel of Figure 6) is due to the dip in the proton spectrum. It results from the intersection of the minimal model and the components from galaxy clusters. Below 10^9 GeV, both the UFA and MPCS models give similar results and can explain the observed spectra. We have also shown the mean logarithmic mass plot for a combination of each different extragalactic model with the two different Galactic components (bottom panel of Figure 6). It is clear from the plot that all these different models for the extragalactic component, in combination with the Galactic components, follow the observed trend of mean logarithmic mass for the whole energy range.

7. Discussion

Our study demonstrates that the CRs originating from spatially distributed young, massive star clusters in the Galactic plane fit well the all-particle CR spectrum, particularly in the 10^7–10^9 GeV energy range, and therefore this can be a potential candidate for the "second Galactic component" of CRs. We also show that the observed all-particle spectrum, as well as the CR composition at high energies, can be explained with the following two types of Galactic sources: (i) SNR-CRs, dominating the spectrum up to $\sim 10^7$ GeV, and (ii) star cluster CRs, which dominate in the range 10^7–10^9 GeV.

The SNR-CR component can only contribute up to maximum energy, corresponding to a proton cutoff energy of 2.5×10^6 GeV (Thoudam et al. 2016). Such a high value of energy cannot be achieved if we consider the DSA mechanism with typical values of the magnetic field in the ISM. However, some numerical simulations have indicated that SN shocks can amplify the magnetic field near them several times larger than the value in the ISM (Bell & Lucek 2001; Reville & Bell 2012). Such a strong magnetic field can accelerate CR protons up to the cutoff energy used in this study. In addition, recently detected γ-rays from a few SNRs have also identified a few SNRs as CR PeVatrons that can accelerate particles up to a few times $\sim 10^6$ GeV energy.

According to our model, the component of CRs, which is plausibly generated in star clusters, can contribute significantly to the total CR flux, especially in the 10^7–10^9 GeV range, if one considers that the protons can be accelerated up to 5×10^7 GeV energy (and for other elements with atomic number Z, the maximum energy is $5 \times 10^7 Z$ GeV) in these young compact star clusters and a CR injection fraction of ∼5%. Note that this value of maximum energy required for protons is slightly on the higher side but can be justified under the assumption of the very high initial shock velocity of SNRs inside compact clusters, faster wind velocity, and possible amplification of magnetic field inside the cluster due to the presence of various instabilities. Note also that the recently detected γ-ray photons by LHAASO in the PeV range from 12 objects, some of which are associated with massive star clusters, have indicated that these clusters can accelerate particles at least up to a few tens of PeV (Cao et al. 2021), consistent with our estimates.

Inside an OB association, individual SNR shocks, as well as colliding shocks, can accelerate particles on a timescale below

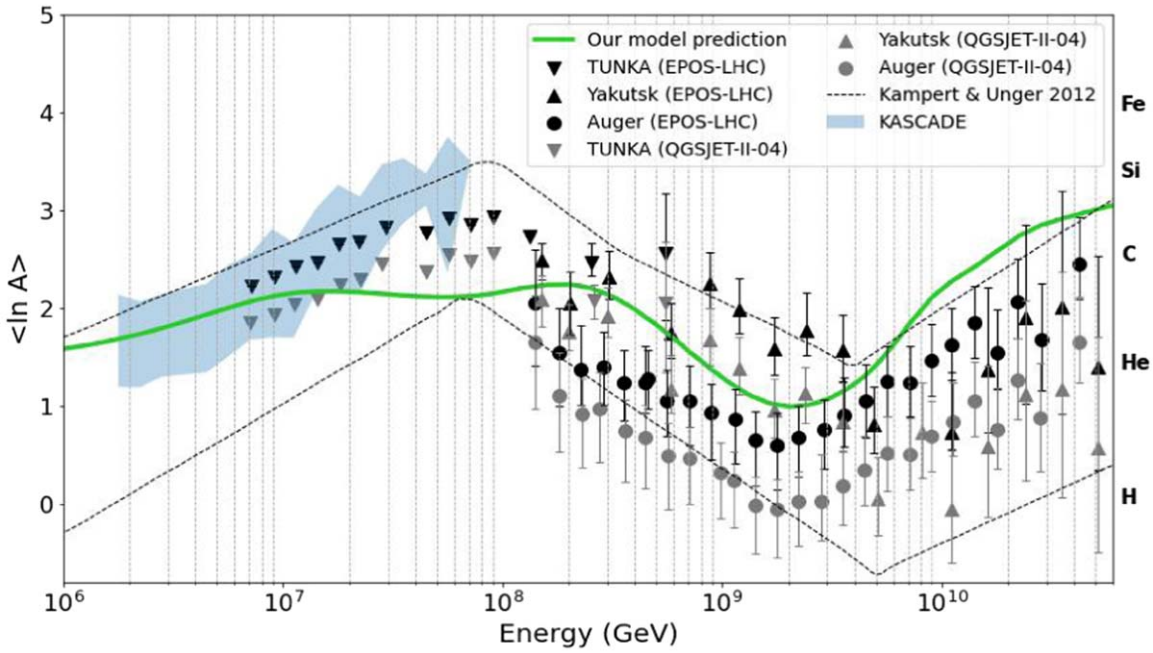

Figure 5. Mean logarithmic mass $\langle \ln A \rangle$ of CRs as a function of energy, predicted using the combination of SNR-CR, CRs from star clusters (these two are Galactic components), and the EG-UFA model (extragalactic component; Unger et al. 2015). Data: KASCADE (Antoni et al. 2005), TUNKA (Berezhnev 2015), Yakutsk (Knurenko & Sabourov 2011), the Pierre Auger Observatory (The Pierre Auger Collaboration et al. 2015), and the different optical measurements compiled in Kampert & Unger (2012). The two different colored (black and gray) sets of data points correspond to the two models EPOS-LHC and QGSJET-II-04, respectively, which have been used to convert $X_{\max}$ values to $\langle \ln A \rangle$ (see Equation (18)).

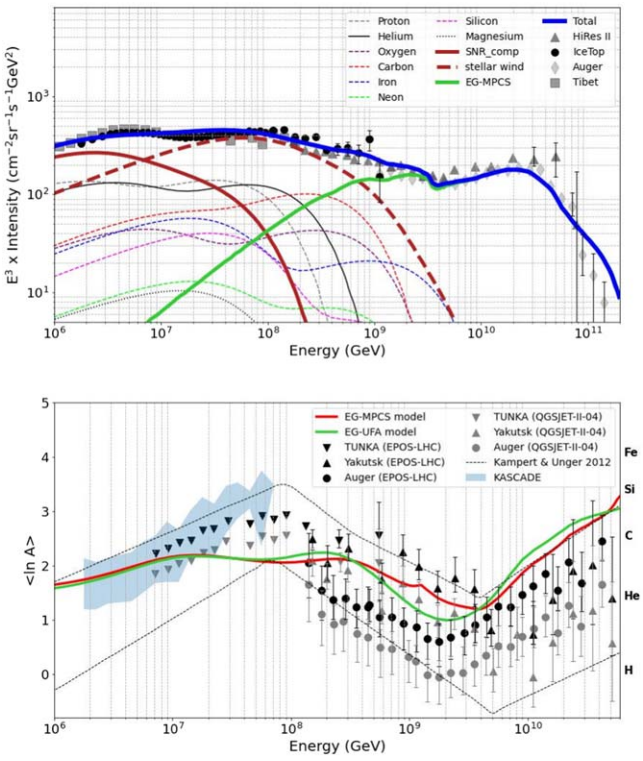

Figure 6. Top panel: all-particle CR spectrum when combined with SNR-CRs and the EG-MPCS model (Rachen 2015) for the extragalactic CRs. Bottom panel: mean logarithmic mass when combined with the EG-MPCS (red curve) and EG-UFA (green curve) models. Data are the same as in Figure 5.

1000 yr. An OB association may enter the evolutionary stage of multiple SN explosions on a timescale larger than a few hundred thousand years. It can create large bubbles of ∼50 pc size, and the injected mechanical power can reach $\sim 10^{38}$ erg s^{-1} over 10 Myr, the lifetime of a superbubble. This process is supplemented by the formation of multiple shocks, large-scale flows, and broad spectra of MHD fluctuations in a tenuous plasma with frozen-in magnetic fields. The collective effect of multiple SNRs and strong winds of young, massive stars in a superbubble is likely to energize CR particles up to hundreds of PeV in energy (see Montmerle 1979; Cesarsky & Montmerle 1983; Bykov & Fleishman 1992; Axford 1994; Higdon et al. 1998; Bykov & Toptygin 2001; Marcowith et al. 2006; Ferrand & Marcowith 2010) and even to extend the spectrum of accelerated particles to energies well beyond the "knee" (Bykov & Toptygin 2001).

Gupta et al. (2020) pointed out the advantage of considering CRs accelerated in massive star clusters in explaining several phenomena (e.g., neon isotope ratio) that are left unexplained by the paradigm of CR production in SNRs. They also proposed that this component need not be considered entirely independent and separate from the SNR component since massive stars (which are the progenitors of SNRs) always form in clusters. Therefore, the two components (SNR-CR and star cluster CRs) arise from similar sources, with some differences. The SNR-CRs can be thought of as CRs produced in individual SNRs, which arise from very small clusters with one or two massive stars, whereas the second component can be thought of as arising from different shocks that occur in the environment of massive star clusters. Hence, the two components can be put on the same platform, and the combined scenario offers a fuller, more complete picture of the phenomenon of CR acceleration in the Galaxy.

Finally, we discuss some caveats of our model. The injection fraction, a free parameter in our analysis whose value is obtained by fitting the all-particle CR spectrum, ultimately depends on many other factors, such as diffusion coefficient,

the assumed lower limit of the number of OB stars in a cluster, and so on. With a higher value of diffusion coefficient, the required injection fraction should be increased in order to match our results with observations. A larger diffusion coefficient implies that particles would diffuse out of the source more rapidly, which will decrease the particle density in the vicinity of clusters. This is why one needs a larger injection fraction to explain the observational data. On the other hand, the total number of OB associations depends on the lower cutoff in the distribution of cluster masses. For example, the number of OB associations that has a minimum of 30 OB stars is lower than the number of OB associations with a minimum of 10 OB stars. For the second case, the required injection fraction will be lower (since the number of OB associations is higher). In addition, the location of the peak of the cluster spatial distribution has a significant effect on the observed flux and may introduce some uncertainty to the value of the injection fraction parameter.

There are other uncertainties that arise from the assumed abundances of the eight elements considered here. This elemental abundance depends on the rotational velocity of the stars. For our calculations, we have used the abundances of stars, which rotate with a velocity that is 60% of the critical velocity of the star. Varying the rotational velocity would change the elemental abundances. This will give an uncertainty between 2% and 3% in the mean logarithmic mass plot (Figure 5). Results may also change if abundances from other previous works (Heger et al. 2000, 2005) were to be used. Comparing the abundances from these works with the ones used here, we find that it would introduce an uncertainty of 5%–7% in Figure 5. However, these variations will not significantly change the shape of our predicted $\langle \ln A \rangle$.

8. Conclusions

In this paper, we suggest that the "second Galactic component of CRs," needed to explain the observed flux of CRs in the range between the "knee" and the "ankle" (10^7–10^9 GeV), may arise from a distribution of massive star clusters.

This component can bridge the gap between the SNR-CR component, which dominates below $\sim 10^7$ GeV, and the extragalactic component, which dominates above $\sim 10^9$ GeV. It has been previously noted that SNR-CRs and CRs from star clusters need not be considered two separate components, but rather originating from similar sources, namely massive star clusters, the less massive ones leading to individual SNRs and SNR-CRs, while the more massive ones can accelerate CRs in a variety of strong shocks appearing in the dense cluster environment. We have argued that there is a possibility of acceleration of protons up to a few tens of PeV by considering the particle acceleration around the WTS, as well as acceleration by SNR shocks inside massive star clusters. This value is larger than that possible in the standard paradigm of CR acceleration inside SNRs present in the ISM. In this paper, we have carried out a detailed calculation of the propagation of CRs in the Galaxy and demonstrated that this model can possibly explain the all-particle CR spectrum measured at Earth. Our calculation considers a realistic distribution of star clusters in the Galaxy and also includes all the important transport processes of CRs, including reacceleration by the old SNRs in the Galaxy.

Our analysis requires a proton cutoff energy of $\sim 5 \times 10^7$ GeV for the CRs accelerated in star clusters. A comparison of our analytical results with the observed all-particle CR spectrum yields an injection fraction (the fraction of kinetic energy of shocks being deposited in CRs) of ∼5% (depending on the choice of the extragalactic component). Furthermore, the variation of the mean logarithmic mass with CR energy (especially in the energy range of around 10^7–10^9 GeV) supports the argument that the suggested CR component from star clusters can be considered as the second Galactic component of CRs.

Acknowledgments

We would like to thank Arpita Roy for the stellar wind elemental abundance data and acknowledge the Australian supercomputer facilities GADI and AVATAR, where those simulations have been run. We thank Manami Roy and Alankar Dutta for the valuable discussions. We also thank Thibault Vieu for the helpful discussions. S.B. acknowledges the Prime Minister's Research Fellowship (PMRF) and Govt. of India for financial support. S.T. acknowledges funding from the Abu Dhabi Award for Research Excellence (AARE19-224) and the Khalifa University Emerging Science & Innovation grant (ESIG-2023-008). P.S. acknowledges a Swarnajayanti Fellowship (DST/SJF/PSA-03/2016-17) and a National Supercomputing Mission (NSM) grant from the Department of Science and Technology, India.

Data Availability

The data not explicitly presented in the paper will be available upon reasonable request from the first author.

ORCID iDs

Sourav Bhadra https://orcid.org/0000-0002-0044-9751

References

Aartsen, M. G., Abbasi, R., Abdou, Y., et al. 2013, PhRvD, 88, 042004
Abeysekara, A. U., Albert, A., Alfaro, R., et al. 2021, NatAs, 5, 465
Ackermann, M., Ajello, M., Allafort, A., et al. 2013, Sci, 339, 807
Adriani, O., Barbarino, G. C., Bazilevskaya, G. A., et al. 2011, Sci, 332, 69
Aguilar, M., Aisa, D., Alpat, B., et al. 2015, PhRvL, 115, 211101
Aharonian, F., Yang, R., & de Oña Wilhelmi, E. 2019, NatAs, 3, 561
Ahn, H. S., Allison, P., Bagliesi, M. G., et al. 2009, ApJ, 707, 593
Aloisio, R., Berezinsky, V., & Blasi, P. 2014, JCAP, 2014, 020
Aloisio, R., Berezinsky, V., & Gazizov, A. 2012, APh, 39, 129
Amenomori, M., Bi, X. J., Chen, D., et al. 2008, ApJ, 678, 1165
An, Q., Asfandiyarov, R., Azzarello, P., et al. 2019, SciA, 5, eaax3793
Antoni, T., Apel, W. D., Badea, A. F., et al. 2005, APh, 24, 1
Axford, W. I. 1994, ApJS, 90, 937
Axford, W. I., Leer, E., & Skadron, G. 1977, ICRC (Budapest), 11, 132
Bagnulo, S., Wade, G. A., Nazé, Y., et al. 2020, A&A, 635, A163
Bell, A. R. 1978, MNRAS, 182, 147
Bell, A. R., & Lucek, S. G. 2001, MNRAS, 321, 433
Berezhnev, S. F. 2015, ICRC (The Hague), 33, 326
Berezinskii, V. S., & Grigor'eva, S. I. 1988, A&A, 199, 1
Berezinsky, V., Gazizov, A., & Grigorieva, S. 2006, PhRvD, 74, 043005
Bhadra, S., Gupta, S., Nath, B. B., & Sharma, P. 2022, MNRAS, 510, 5579
Biermann, P. L., & Cassinelli, J. P. 1993, A&A, 277, 691
Binns, W. R., Wiedenbeck, M. E., Arnould, M., et al. 2008, NewAR, 52, 427
Blandford, R. D., & Ostriker, J. P. 1978, ApJL, 221, L29
Blasi, P. 2013, A&ARv, 21, 70
Blazère, A., Neiner, C., Tkachenko, A., Bouret, J. C., & Rivinius, T. 2015, A&A, 582, A110
Bloemen, J. B. G. M., Dogiel, V. A., Dorman, V. L., & Ptuskin, V. S. 1993, A&A, 267, 372
Breitschwerdt, D., Dogiel, V. A., & Völk, H. J. 2002, A&A, 385, 216

Bronfman, L., Casassus, S., May, J., & Nyman, L. Å 2000, A&A, 358, 521
Bustard, C., Zweibel, E. G., & Cotter, C. 2017, ApJ, 835, 72
Bykov, A. M. 2014, A&ARv, 22, 77
Bykov, A. M., & Fleishman, G. D. 1992, MNRAS, 255, 269
Bykov, A. M., Marcowith, A., Amato, E., et al. 2020, SSRv, 216, 42
Bykov, A. M., & Toptygin, I. N. 2001, AstL, 27, 625
Cao, Z., Aharonian, F. A., An, Q., et al. 2021, Natur, 594, 33
Caprioli, D. 2015, ICRC (The Hague), 34, 8
Caprioli, D., Blasi, P., & Amato, E. 2011, APh, 34, 447
Cesarsky, C. J., & Montmerle, T. 1983, SSRv, 36, 173
di Matteo, A. 2015, ICRC (The Hague), 34, 249
Drury, L. O., Aharonian, F. A., & Voelk, H. J. 1994, A&A, 287, 959
Engelmann, J. J., Ferrando, P., Soutoul, A., et al. 1990, A&A, 233, 96
Fermi, E. 1949, PhRv, 75, 1169
Ferrand, G., & Marcowith, A. 2010, A&A, 510, A101
Gabici, S., Evoli, C., Gaggero, D., et al. 2019, IJMPD, 28, 1930022
Greisen, K. 1966, PhRvL, 16, 748
Gupta, S., Nath, B. B., & Sharma, P. 2018, MNRAS, 479, 5220
Gupta, S., Nath, B. B., Sharma, P., & Eichler, D. 2020, MNRAS, 493, 3159
Heger, A., Langer, N., & Woosley, S. E. 2000, ApJ, 528, 368
Heger, A., Woosley, S. E., & Spruit, H. C. 2005, ApJ, 626, 350
H. E. S. S. Collaboration, Abdalla, H., Abramowski, A., et al. 2018, A&A, 612, A6
Higdon, J. C., Lingenfelter, R. E., & Ramaty, R. 1998, ApJL, 509, L33
High Resolution Fly'S Eye Collaboration, Abbasi, R. U., Abu-Zayyad, T., et al. 2009, APh, 32, 53
Hillas, A. M. 1967, PhLA, 24, 677
Hörandel, J. R. 2003, JPhG, 29, 2439
Jokipii, J. R., & Morfill, G. 1987, ApJ, 312, 170
Jones, F. C., Lukasiak, A., Ptuskin, V., & Webber, W. 2001, ApJ, 547, 264
Kampert, K.-H., & Unger, M. 2012, APh, 35, 660
Kang, H., Ryu, D., & Jones, T. W. 1996, ApJ, 456, 422
Kelner, S. R., Aharonian, F. A., & Bugayov, V. V. 2006, PhRvD, 74, 034018
Knödlseder, J. 2013, in Cosmic Rays in Star-Forming Environments, ed. D. F. Torres & O. Reimer (Berlin: Springer), 169
Knurenko, S. P., & Sabourov, A. 2011, ASTRA, 7, 251
Krymskii, G. F. 1977, DoSSR, 234, 1306
Lagage, P. O., & Cesarsky, C. J. 1983, A&A, 125, 249
Lerche, I., & Schlickeiser, R. 1982, A&A, 116, 10
Longmore, S. N., Kruijssen, J. M. D., Bastian, N., et al. 2014, in Protostars and Planets VI, ed. H. Beuther et al. (Tucson, AZ: Univ. of Arizona Press), 291
Mannheim, K., Protheroe, R. J., & Rachen, J. P. 2000, PhRvD, 63, 023003
Marcowith, A., Lemoine, M., & Pelletier, G. 2006, A&A, 453, 193
Montmerle, T. 1979, ApJ, 231, 95
Morlino, G. 2017, in Handbook of Supernovae, ed. A. W. Alsabti & P. Murdin (Berlin: Springer), 1711
Mueller, D., Swordy, S. P., Meyer, P., L'Heureux, J., & Grunsfeld, J. M. 1991, ApJ, 374, 356
Nath, B. B., & Eichler, D. 2020, MNRAS, 499, L1
Neiner, C., Grunhut, J., Leroy, B., De Becker, M., & Rauw, G. 2015, A&A, 575, A66
Obermeier, A., Ave, M., Boyle, P., et al. 2011, ApJ, 742, 14
Oey, M. S., & Clarke, C. J. 1997, MNRAS, 289, 570
Panov, A. D., Adams, J. H. J., Ahn, H. S., et al. 2007, BRASP, 71, 494
The Pierre Auger Collaboration, Aab, A., Abreu, P., et al. 2013, arXiv:1307.5059
The Pierre Auger Collaboration, Aab, A., Abreu, P., et al. 2015, arXiv:1509.03732
Rachen, J. 2015, in Proc. Texas Symp. on Relative Astrophysics 28, 230
Rachen, J. P., & Biermann, P. L. 1993, A&A, 272, 161
Reville, B., & Bell, A. R. 2012, MNRAS, 419, 2433
Roy, A., Dopita, M. A., Krumholz, M. R., et al. 2021, MNRAS, 502, 4359
Salpeter, E. E. 1955, ApJ, 121, 161
Sarkar, K. C., Nath, B. B., Sharma, P., & Shchekinov, Y. 2015, MNRAS, 448, 328
Strong, A. W., & Moskalenko, I. V. 1998, ApJ, 509, 212
Suzuki, H., Bamba, A., Yamazaki, R., & Ohira, Y. 2022, ApJ, 924, 45
Taillet, R., & Maurin, D. 2003, A&A, 402, 971
Tatischeff, V., Raymond, J. C., Duprat, J., Gabici, S., & Recchia, S. 2021, MNRAS, 508, 1321
Thoudam, S., & Hörandel, J. R. 2014, A&A, 567, A33
Thoudam, S., Rachen, J. P., van Vliet, A., et al. 2016, A&A, 595, A33
Tibet ASγ Collaboration, Amenomori, M., Bao, Y. W., et al. 2021, NatAs, 5, 460
Unger, M., Farrar, G. R., & Anchordoqui, L. A. 2015, PhRvD, 92, 123001
Vieu, T., & Reville, B. 2023, MNRAS, 519, 136
Vieu, T., Reville, B., & Aharonian, F. 2022, MNRAS, 515, 2256
Wandel, A., Eichler, D., Letaw, J. R., Silberberg, R., & Tsao, C. H. 1987, ApJ, 316, 676
Waxman, E. 1995, PhRvL, 75, 386
Weaver, R., McCray, R., Castor, J., Shapiro, P., & Moore, R. 1977, ApJ, 218, 377
Webb, G. M., Axford, W. I., & Forman, M. A. 1985, ApJ, 298, 684
Wiedenbeck, M. E., Binns, W. R., Christian, E. R., et al. 1999, ApJL, 523, L61
Yoon, Y. S., Ahn, H. S., Allison, P. S., et al. 2011, ApJ, 728, 122
Zatsepin, G. T., & Kuz'min, V. A. 1966, JETPL, 4, 78
Zirakashvili, V. N., & Völk, H. J. 2006, AdSpR, 37, 1923